Available online at www.sciencedirect.com
SCIENCE DIRECT®
Journal of Power Sources 119–121 (2003) 755–759
JOURNAL OF POWER SOURCES
www.elsevier.com/locate/jpowsour

Experimental and computational study of the structure and electrochemical properties of monoclinic $Li_xM_2(PO_4)_3$ compounds

D. Morgan[a,*], G. Ceder[a,b], M.Y. Saïdi[c], J. Barker[c], J. Swoyer[c], H. Huang[c], G. Adamson[c]

[a]*Computational Modeling Consultants, Wellesley, MA, USA*
[b]*Massachusetts Institute of Technology, Cambridge, MA, USA*
[c]*Valence Technology Inc., Henderson, NV, USA*

Abstract

This paper presents a combined computational and experimental study of the structural and electrochemical properties of monoclinic $Li_xM_2(PO_4)_3$ (with a focus on M = V). The voltage curve for $x = 0$–3 Li is measured experimentally and calculated. Features of the voltage curve are understood as emerging from site energetics, Li ordering, and redox couples. These features are found to be largely independent of alloying and a simple additive model is proposed to analyze the voltage curve for different cation substitutions. The model is shown to be very useful for understanding experimental results for a number of substituted compounds.

Keywords: $Li_xM_2(PO_4)_3$; NASICON; Li-battery

1. Introduction

Phosphates form a class of potentially very interesting positive electrode materials for rechargeable Li batteries. Many phosphates form structures similar to the NASICON fast Na conductor [1]. In this structure, SiO_4 groups link metal-oxygen octahedra in a three-dimensional network. NASICON-like phosphates generally have better electronic conductivity than silicates but also allow rapid conduction of alkali cations. In addition, the phosphates are extremely stable, even for changes in alkali-to-metal ratios larger than 1. This has offered the prospect of inexpensive, safe, and stable positive electrode materials.

There has been extensive work characterizing NASICON-like phosphates and demonstrating that they can be used as intercalation compounds [2–9]. It was recently shown that three Li could be extracted from $Li_3V_2(PO_4)_3$ [10,11]. The reversible cycling of all Li from $Li_3V_2(PO_4)_3$ would correspond to a theoretical capacity of 197 mAh/g. Considering the very good stability of these materials and the voltage range of operation, this performance suggests these compounds could make commercially useful positive electrode materials.

In this paper we use a combination of experimental and computational methods to characterize the structure and electrochemical properties of $Li_xM_2(PO_4)_3$ phosphates (with a focus on M = V) with the monoclinic structure. By combining experimental results with the results of first-principles computations we are able to show how the voltage curve features can be traced back to the crystallographic and electronic structure. This understanding leads to a heuristic model to predict the potential curve for a variety of metal-substituted phosphates. A more detailed discussion of this work can be found in [12]. Many of the issues discussed in this paper have recently been investigated experimentally by Yin et al. [13]. Unfortunately, the work by Yin et al. was published after the final version of this manuscript had been accepted, so they are not discussed further here.

2. Experimental methods and results

The monoclinic lithium vanadium phosphate was prepared by mixing stoichiometric amounts of $NH_4H_2PO_4$, V_2O_5 and Li_2CO_3 (Alfa-Aesar, Ward Hill, MA). The mixture

* Corresponding author. Present address: Department of Materials Science and Engineering, Massachusetts Institute of Technology, 77 Massachusetts Avenue, Cambridge, MA 02139-4307, USA.
Tel.: +1-617-252-1507; fax: +1-617-258-6534;
mobile: +1-617-733-9723.
E-mail address: dmorgan@mit.edu (D. Morgan).

0378-7753/03/$ – see front matter © 2003 Elsevier Science B.V. All rights reserved.
doi:10.1016/S0378-7753(03)00216-7

was initially heated to 300 °C in air for 4 h to allow H_2O and NH_3 to evolve. The resulting product was then ground, pelletized and heated to 850 °C under a stream of pure hydrogen for 8 h in a sealed tube furnace. Once the furnace had cooled to room temperature, the pellet was crushed and prepared for electrode processing. Equivalent monoclinic compounds, based on mixtures of V/Ti, V/Cr, and V/Al couples were prepared in the same manner where the vanadium was partially replaced by an alternative metal oxide. Powder X-ray diffraction was used to confirm that the material was a highly crystalline phase with no detectable impurities.

$Li_3V_2(PO_4)_3$ electrodes were prepared by mixing with a conductive carbon, Super P (Erachem, Belgium), and a binder, PVDF-HFP copolymer (Kynar 2801, Alfatochem). The electrode constituents were mixed into a slurry with acetone to achieve homogeneity. The resulting slurry was coated onto a glass plate using a doctor blade. After the acetone had evaporated, the resulting electrode composition was 80:10:10 of active material, carbon and binder respectively. The electrode was then dried and transferred into an argon-filled glove box for cell assembly. The electrode was cut into a 0.75 in. diameter disc and placed on top of an aluminum foil current collector. Glass fiber separator was placed between the $Li_3V_2(PO_4)_3$ positive electrode and lithium metal, pressed onto a copper current collector, as the anode. The electrolyte used consisted of a 1M solution of $LiPF_6$ in a mixture 2:1 by weight of ethylene carbonate (EC) and dimethyl carbonate (DMC), (Grant-Ferro, Louisiana).

Voltage traces were collected using the electrochemical voltage spectroscopy (EVS) technique [14,15]. The conditions chosen for the cell cycling were voltage limits between 3.0 and 4.2 V (versus Li/Li^+), voltage step sizes of 10 mV and critical current density <100 $\mu A/cm^2$. These conditions were chosen so as to maintain the system close to thermodynamic equilibrium throughout the discharge/charge cycle. As such, the voltage profile should provide a close approximation to the open cell voltage (OCV)–composition relationship.

3. Computational methods

All calculations were performed in the local density approximation (LDA) to density functional theory as implemented in the Vienna *Ab Initio* Simulation Package (VASP) [16,17]. The nuclei and core electrons were represented with ultra-soft pseudo-potentials and all structures were fully relaxed with respect to internal and external cell parameters and atomic positions, unless explicitly stated. The wave functions were expanded in plane waves with kinetic energy below 405 eV and Brillouin zone integration of the band structure was performed at the gamma point. The calculations were ferromagnetically spin-polarized. This is an approximation, since most oxide systems are antiferromagnetic. However, the metal atoms in these materials are quite far apart, and our calculations and previous experiments [18] suggest that magnetic interactions are fairly weak in these systems.

4. Li Sites in the monoclinic structure

In order to study the voltage curve for the monoclinic structure it is necessary to identify potential alkali cation sites. The monoclinic structure of $A_xM_2(PO_4)_3$ contains lantern unit motifs at angles to each other, which makes the locations of the A cations difficult to describe. A schematic picture is shown in Fig. 1. Some of the most extensive monoclinic structural information comes from the study of $Li_3Fe_2(PO_4)_3$ by Bykov et al. [19] and we will make use of these results to establish potential Li locations. The $Li_3Fe_2(PO_4)_3$ structure undergoes two phase changes upon

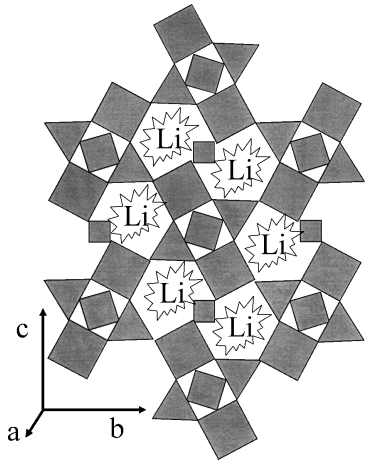

Fig. 1. Schematic picture of the monoclinic structure with approximate area of Li positions identified.

Table 1
Site environments of the alkali ion in the monoclinic structure in α, β and γ phases

Sites	Wykoff	Occupied	Coordinated	Equivalent sites
$P12_1/n1$				
α1	4e	1	4 (regular tetrahedron)	≈γ1A
α2	4e	1	5 (distorted trigonal bipyramid)	≈γ2A
α3	4e	1	5 (distorted trigonal bipyramid)	≈α3
$P12_1/n1$				
β1	4e	1	4 (regular tetrahedron)	≈γ1A
β2	4e	1	5 (distorted trigonal bipyramid)	≈γ2A
β3	4e	1	4 (regular tetrahedron)	≈γ1B
Pbcn				
γ1	8d	1	4 (regular tetrahedron)	≈γ1A
γ2	8d	0.25	5	≈γ2A
γ3	8d	0.25	4	≈γ3A

All data taken from [19] and references therein. The symbol (≈) will be used to denote sites that are in very similar environments.

heating. The three phases are designated, in order of appearance with increasing temperature, by α, β, and γ. They have symmetry groups $P2_1/n$ (space group number 14) for α and β, and *Pbcn* (space group number 60) for γ. There are three symmetry inequivalent sites occupied in each phase, which we will label with 1, 2, or 3. Viewed from the $P2_1/n$ space group the gamma sites split into two groups, which we will label A and B. This gives a total of 12 potential sites, α1–3, β1–3, γ1–3A, and γ1–3B.

Fortunately, a careful examination of these sites shows that many have very similar environments and can be considered equivalent. It can be shown that there are really only four distinct Li sites: γ1A, γ2A, γ3A, and α3. Some basic characteristics of the Li sites based on experimental data, including the site equivalences, are shown in Table 1.

5. Computational results

5.1. Open circuit voltage curve

The experimental open circuit voltage curve for $Li_xV_2(PO_4)_3$ is shown in Fig. 2. We have calculated the $T = 0$ voltage curve from first-principles, using standard methods [20], and it is also shown in Fig. 2. The calculated voltages have been shifted by an overall constant (+1.75 V) to match the experimental value at $x = 3$ (the origin of this overall voltage error is not known). The experimental results have been scaled so that the total removed capacity corresponds to 3 Li.

The calculated curve reproduces the main features of the experimental charge curve. In particular, the steps at $x = 2.5$, 2, and 1. There are a number of other small steps in the calculated curve which do not seem to appear in the experiments. These steps are fairly weak, and may be absent in the experiments because they are washed out by thermal effects at room temperature. The extra steps may also be due to errors in the calculation methods, most likely the local density approximation. The calculations can be used to determine the origin of the three main features of the experimental charge curve. In the following, all results refer to the $Li_xV_2(PO_4)_3$ material unless otherwise stated.

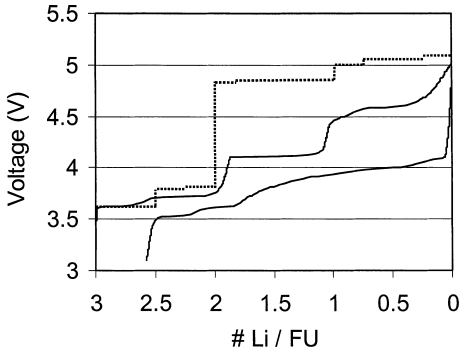

Fig. 2. Comparison of room temperature experimental (solid line) and $T = 0$ K calculated (dashed line) voltage curve for $Li_xV_2(PO_4)_3$.

Table 2
Relative stability of isolated Li in candidate mono sites

$x = 0.25$, $Li_{0.25}M_2(PO_4)_3$, E (meV per Li)	γ1A	γ2A	γ3A	α3
V	0	230	80	110
Fe	0	170	200	280

The site energies for isolated Li, relative to the γ1 site energy, are shown in Table 2. The results indicate that the γ1 position is the most stable site for both V and Fe. These stable sites are tetrahedrally coordinated with oxygen (see Table 1), which we believe is key to their high stability. While there is no experimental information concerning site occupations at low lithium concentration for these materials, our results are consistent with the experimental finding that the tetrahedral γ1 sites are fully occupied in the gamma phase of $Li_3Fe_2(PO_4)_3$ [19].

At $x = 1$ our calculations suggest that the Li occupy the tetrahedral α1 sites (see Section 4). This is consistent with the occupation of α sites in the low-temperature $Li_3Fe_2(PO_4)_3$ alpha phase as well as the stability of tetrahedral sites seen in Table 2. With only α1 sites occupied the structure is monoclinic. Although there may be some Li ordering effect at this concentration, the most obvious cause of the step in voltage is that the redox couple for V changes from 3+/4+ to 4+/5+.

At $x = 2$ our calculations suggest that all the tetrahedral γ1 sites are filled. This creates a very stable structure that has orthorhombic symmetry. It is the stability of these fully occupied tetrahedral sites that creates the large step seen at $x = 2$.

At $x = 2.5$ our calculations find a significant ordering tendency in the Li, giving rise to the step at this composition. The exact nature of the ordered phase was not determined but calculations suggest that it has filled γ1 sites, with extra Li occupying the γ2 and γ3 sites. This would make the $x = 2.5$ ordering more like the $x = 2$ structure with added Li than the $x = 3$ structure with missing Li.

The calculated voltage step at $x = 2$ is about 2.5× larger than the experimentally measured value. This discrepancy could be due to the electronic structure method we used or because we might have not used the lowest energy structure for $Li_1V_2(PO_4)_3$. Finding a lower energy state for $Li_1V_2(PO_4)_3$ would also increase the difference of the average voltage for the $V^{3+/4+}$ and $V^{4+/5+}$ redox couple and bring it in closer agreement with experiment. It is possible that at least some V ions move to more stable non-octahedral environments as they become oxidized to 4+ or 5+. It is well known that V^{5+} is often found in distorted octahedral or non-octahedral sites (e.g. in V_2O_5). In addition, our experiments on V systems cycled in the range $x = 1-3$ often yield yellow coloration at $x = 1$, which is evidence of V^{5+}.

This presence of V^{5+} in a nominally V^{4+} average charge state suggests that charge disproportionation ($2V^{4+} \rightarrow V^{3+} + V^{5+}$) may be occurring. Charge disproportionation would be facilitated by the shifting of some V

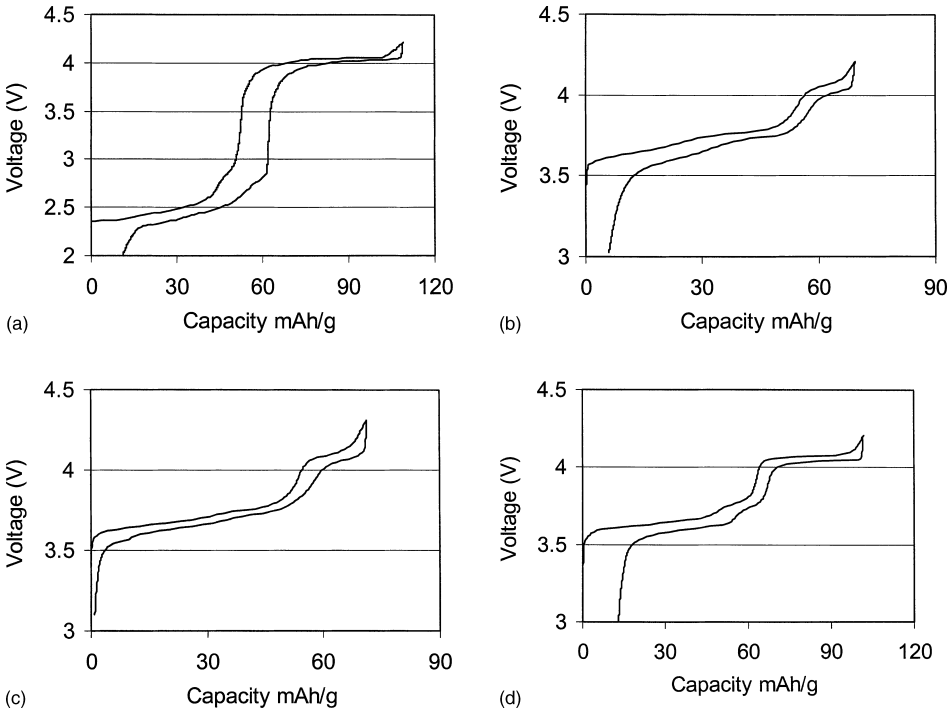

Fig. 3. Experimental voltage curves for doped $Li_3M_2(PO_4)_3$: (a) M_2 = TiV, (b) M_2 = AlV, (c) M_2 = CrV, (d) $M_2 = Al_{0.5}V_{1.5}$.

(presumably the V^{5+}) to non-octahedral sites. Finally, in the cases where the system is cycled to $x < 1$ (creating V^{5+}) the discharge looks very different from the charge, particularly for $x < 1$. This suggests that the system has undergone significant structural changes during charging. These structural changes might consist of shifting V^{5+} into non-octahedral environments. However, at this time we are aware of no direct experimental measurements showing V shifting into non-octahedral sites in this material.

The above discussion has focused on comparing our calculations to the experimental charge curve, since the discharge curve looks quite different in the range $x = 0 \rightarrow 2$. We believe that during discharge from $x = 0$ there is initially a structural change that creates significantly different Li environments than those seen upon charging. The nature of this structural change has not been identified and is not presently included in the calculations. It is interesting to note that the structural transformation which occurs on cycling $x = 3 \rightarrow 0$ does not occur if the materials is cycled from $x = 3 \rightarrow 1$.

5.1.1. Doped materials

The previous analysis allows us to understand and approximately predict the OCV curve for all materials with the monoclinic NASICON-like structure, for any chemistry on the transition metal site. The shape of the OCV curve is determined by the sum of the energy for Li^+ removal and the energy for oxidation of the transition metal(s). Li ordering and site selection will always impose features at $x = 2.5$ (≈30 mAh/g) and $x = 2$ (≈60 mAh/g). These are respectively due to ordering and to a switch between Li removal from non-tetrahedral sites to tetrahedral sites.

Fig. 3a–d show, respectively, the voltage curves for $Li_x(VTi)(PO_4)_3$, $Li_x(VAl)(PO_4)_3$, $Li_x(VCr)(PO_4)_3$ and $Li_x(V_{1.5}Al_{0.5})(PO_4)_3$. In Fig. 3a the Ti^{3+}/Ti^{4+} couple is active first during charge, which creates the initial region at about 2.5 V. Near $x = 2$ (≈60 mAh/g) both the sites from which Li is removed and the active redox couple change, creating a very large step to about 4 V. The rapid increase in voltage near ≈50 mAh/g is probably due to the removal of Li from tetrahedral sites but with electrons from the Ti^{3+}/Ti^{4+} redox couple, indicating that some non-tetrahedral Li cannot be removed, or that some of these sites were not filled in the first place.

Neither Cr nor Al is active, so the remaining curves b–d are all produced solely by V activity. These voltage curves are therefore similar to pure V, except truncated in proportion to the amount of V remaining. In Fig. 3b and c there is a small plateau near 4 V at the end of charge. We believe that this corresponds to the removal of Li from tetrahedral sites with the V^{3+}/V^{4+} redox couple. Perhaps some of the non-tetrahedral Li cannot be removed because it is in regions with low V content.

6. Conclusion

We have combined computational and experimental results to understand the voltage curve in monoclinic structures. We have focused on the $Li_xV_2(PO_4)_3$ material but many of the results have been shown to apply to the monoclinic structure in general. The distinctive features in the charge curve were identified to be due to Li ordering ($x = 2.5$), Li site energetics (and Li–Li interactions) ($x = 2$), and redox couple ($x = 1$).

The step due to the redox couple change will occur at different stages of the charge curve depending on the specific metal content.

These underlying mechanisms largely explain the shape and features of a number of doped V compounds. The Li energetics and electron energies operate almost independently and the OCV curve is shaped by the sum of the two effects. We also find that the transition metals do not interact strongly when mixed in the NASICON-like materials and that the voltage of the redox couples in substituted compounds is similar to that in the pure materials. This is consistent with the large separation of the metal cations.

Although we have focused on V, the qualitative aspects of the features of the OCV curve should apply to other chemistries, as they arise from the geometry of the materials and the redox states of the metals. Identifying general characteristics in these materials is particularly important since many substitutions of both metal cations, intercalated cations, and anion units are possible. The features and their origins that we have identified can provide guidance for future investigations into this large class of promising materials.

References

[1] J.B. Goodenough, H.Y.P. Hong, J.A. Kafalas, Mater. Res. Bull. 11 (1976) 203.
[2] C. Delmas, F. Cherkaoui, A. Nadiri et al., Mater. Res. Bull. 22 (1987) 631.
[3] C. Delmas, F. Cherkaoui, P. Hagenmuller, Mater. Res. Bull. 21 (1986) 469.
[4] D. Beltran Porter, R. Olazcuaga, C. Delmas et al., Revue de Chim. Minerale 17 (1980) 458.
[5] L. Abello, K. Chhor, M. Barj et al., J. Mater. Sci. 24 (1989) 3380.
[6] C. Delmas, A. Nadiri, J.L. Soubeyroux, Solid State Ionics 28–30 (1988) 419.
[7] A.K. Padhi, K.S. Nanjundaswamy, C. Masquelier et al., J. Electrochem. Soc. 144 (1997) 2581.
[8] K.S. Nanjundaswamy, A.K. Padhi, J.B. Goodenough et al., Solid State Ionics, Diffusion Reactions 92 (1996) 1.
[9] J. Barker, M.Y. Saïdi, US Patent 5,871,866, (1999).
[10] M.Y. Saïdi, J. Barker, H. Huang et al., Electrochem. Solid State Lett. 5 (2002) A149.
[11] H. Huang, S.C. Yin, T. Kerr, et al., Advanced Mater. 14 (21) (2002) 1525.
[12] D. Morgan, G. Ceder, M.Y. Saïdi, et al., Chem. Mater. 15 (1) (2003) 63–67.
[13] S.-C. Yin, H. Grondey, P. Strobel, et al., J. Am. Chem. Soc. 125 (2003) 326.
[14] A. Thompson, Phys. Rev. Lett. 23 (1978) 1511.
[15] J. Barker, Synth. Met. 32 (1989) 43.
[16] G. Kresse, J. Hafner, Phys. Rev. B 49 (1994) 14251.
[17] G. Kresse, J. Furthmüller, Comput. Mater. Sci. 6 (1996) 15.
[18] G. Rousse, J. Rodriguez-Carvajal, C. Wurm et al., Chem. Mater. 13 (2001) 1527.
[19] A.B. Bykov, A.P. Chirkin, L.N. Demyanets et al., Solid State Ionics 38 (1990) 31.
[20] M.K. Aydinol, G. Ceder, J. Electrochem. Soc. 144 (1997) 3832.